THE JOURNAL OF BIOLOGICAL CHEMISTRY VOL. 291, NO. 15, pp. 7902–7914, April 8, 2016

Membrane Oxidation Enables the Cytosolic Entry of Polyarginine Cell-penetrating Peptides*

Received for publication, December 21, 2015, and in revised form, February 11, 2016 Published, JBC Papers in Press, February 17, 2016, DOI 10.1074/jbc.M115.711564

Ting-Yi Wang, Yusha Sun, Nandhini Muthukrishnan, Alfredo Erazo-Oliveras, Kristina Najjar, and Jean-Philippe Pellois[1]

From the Department of Biochemistry and Biophysics, Texas A&M University, College Station, Texas 77843-2128

Arginine-rich peptides can penetrate cells and consequently be used as delivery agents in various cellular applications. The activity of these reagents is often context-dependent, and the parameters that impact cell entry are not fully understood, giving rise to variability and limiting progress toward their usage. Herein, we report that the cytosolic penetration of linear polyarginine peptides is dependent on the oxidation state of the cell. In particular, we find that hypoxia and cellular antioxidants inhibit cell penetration. In contrast, oxidants promote cytosolic cell entry with an efficiency proportional to the level of reactive oxygen species generated within membranes. Moreover, an antibody that binds to oxidized lipids inhibits cell penetration, whereas extracellularly administered pure oxidized lipids enhance peptide transport into cells. Overall, these data indicate that oxidized lipids are capable of mediating the transport of polyarginine peptides across membranes. These data may also explain variability in cell-penetrating peptide performance in different experimental conditions. These new findings therefore provide new opportunities for the rational design of future cell-permeable compounds and for the optimization of delivery protocols.

Cell-penetrating peptides (CPPs)[2] are useful tools to probe and manipulate cellular processes. They include stapled peptides (1, 2), cyclic peptides (3–6), or peptide analogs, such as peptoids (7–11), that can affect intracellular targets by interfering with protein-protein interactions. The prototypical class of CPPs is the arginine-rich peptides, best represented by R9 or HIV TAT CPPs (12). These agents are typically used as carriers of a wide variety of biologically active cargos (13, 14). Despite their promise of broad utility, the general rules of cytosolic penetration have not yet clearly been established. Delivery efficiencies are often sub-optimal, and in the absence of mechanistic insights, designing better tools often relies on a process of trials and errors. Fundamentally, the properties allowing hydrophilic CPPs to transit across membranes and into cells are not understood, frustrating the adoption or optimization of these compounds in a wide array of applications.

In some instances, cytosolic penetration appears to involve direct plasma membrane translocation (15–18). Alternatively, a two-step process of endocytosis followed by escape from endosomes has also been observed (19–22). It is currently plausible that CPPs utilize these two distinct routes of cellular entry to various degrees. However, the parameters that control cytosolic penetration by one pathway or the other remain unclear. Additionally, the molecular details that explain how a peptide crosses cellular membranes are still lacking. A wide variety of translocation models has been proposed, most of which highlight the ability of CPPs to interact with lipid bilayers (18, 23–29). These mechanisms, although potentially non-exclusive, remain a matter of debate. This is in part because results obtained with CPPs are often unpredictable with high variability in cytosolic penetration. In particular, minor changes in experimental conditions can impact the results obtained, indicating that unknown variables modulate this process.

It is well appreciated that oxidation occurs during typical tissue culture growth conditions and that oxidized lipids and proteins are physiologically relevant components of cellular membranes (30, 31). In principle, the relative abundance of these species varies depending on the level of oxidative stress affecting cells and on the efficiency of various repair mechanisms. Membrane oxidation has already been shown to affect transport processes such as viral infection, the diffusion of small molecule drugs across lipid bilayers, or electroporation (32–34). Based on these observations, we postulated that membrane oxidation might also modulate the cytosolic penetration of CPPs. We establish that the cytosolic penetration of a CPP containing 13 arginine residues is correlated to the oxygen tension used during cell growth and to the presence of oxidants or antioxidants. These effects are more pronounced with a shorter CPP containing 9 arginines, indicating that membrane oxidation is required to achieve penetration with CPPs of low potency. We also establish that extracellular addition of PGPC and PazePC, two oxidized products of phosphatidylcholine, enhances the cytosolic penetration of the Arg_{13} CPP. In contrast, an antibody directed against oxidized phosphatidylcholine species can inhibit cell penetration of this peptide. Together, these results indicate that membrane oxidation is an

* This work was supported by National Institutes of Health Grant R01GM110137 from NIGMS. The authors declare that they have no conflicts of interest with the contents of this article. The content is solely the responsibility of the authors and does not necessarily represent the official views of the National Institutes of Health.

[1] To whom correspondence should be addressed: Dept. of Biochemistry and Biophysics, Texas A&M University, Biochemistry and Biophysics Bldg., Rm. 430, 300 Olsen Blvd., College Station, TX 77843-2128. Tel.: 979-845-0101; Fax: 979-862-4718; E-mail: pellois@tamu.edu.

[2] The abbreviations used are: CPP, cell-penetrating peptide; DEAC, 7-diethylaminocoumarin-3-carboxylic acid; PGPC, 1-palmitoyl-2-glutaryl-*sn*-glycero-3-phosphocholine; DOPC, 1,2-dioleoyl-*sn*-glycero-3-phosphocholine; PazePC, 1-palmitoyl-2-azelaoyl-*sn*-glycero-3-phosphocholine; TMR, 5(6)-carboxytetramethylrhodamine; Fmoc, *N*-(9-fluorenyl)methoxycarbonyl; DPPP, diphenyl 1-pyrenylphosphine; HDF, human dermal fibroblast; Ex, excitation; Em, emission; RFP, red fluorescent protein; Ox-PC, oxidation of phosphatidylcholine.

integral aspect of the cellular penetration process and that certain oxidized components might act as direct CPP transporters.

Experimental Procedures

Peptide Synthesis and Purification—All peptides were synthesized and purified as reported previously (20, 35). Briefly, Fmoc-Arg(pbf)-OH, Fmoc-D-Arg(pbf)-OH, or Fmoc-D-Lys-(Boc)-OH (Novabiochem) was coupled and extended on the Rink-amide MBHA resin (Novabiochem) using Fmoc chemistry-based solid-phase peptide synthesis standard protocol. The fluorophore 5(6)-carboxytetramethylrhodamine (TMR) (Novabiochem) or 7-diethylaminocoumarin-3-carboxylic acid (DEAC) (AnaSpec) was conjugated to the N-terminal amino group of peptide after Fmoc deprotection. The fluorophore-labeled peptides were analyzed and purified by reverse-phase HPLC Agilent 1200 Series system (Agilent) using Vydac C18 column (5-μm particle size, 4 × 150 mm). The correct identity of peptides was confirmed by MALDI-TOF mass spectrometry analysis (Shimadzu) as follows: TMR-r13 (TMR-rrrrrrrrrrrrr-NH_2), expected mass 2460.94 and observed mass 2463.48; TMR-r11 (TMR-rrrrrrrrrr-NH_2), expected mass 2147.29 and observed mass 2148.92; TMR-r9 (TMR-rrrrrrrrr-NH_2), expected mass 1835.09 and observed mass 1835.43; DEAC-k5 (DEAC-kkkkk-NH_2), expected mass 900.59 and observed mass 900.84. TMR-Rn (n = 5–13), DEAC-K9, and dfTAT peptides were obtained by following published protocols (20, 35).

Cell Lines and Cell Culture—Human dermal fibroblast (HDF) (ATCC PCS-201-010) and MCH58 (human skin fibroblast, obtained from E. Shoubridge, Montreal Neurological Institute and Hospital) were cultured in Dulbecco's minimum essential medium (DMEM) (HyClone) supplemented with 10% fetal bovine serum (FBS) (HyClone) and 1× penicillin/streptomycin (MP Biomedicals) (36). For standard cultures (20% oxygen), cells were placed in an incubator (NuAire) with humidified ambient atmosphere containing 5% carbon dioxide at 37 °C. Alternatively, for hypoxic cultures (2% oxygen), cells were cultured in a closed chamber (modular incubator chamber, Billups-Rothenberg, Del Mar, CA). The chamber was purged with humidified 2% oxygen, 5% carbon dioxide, and 93% nitrogen (Praxair) at 20 liters/min for 4 min. The chamber was then sealed and placed in a 37 °C incubator. Cells were subcultured under a normoxic (20% oxygen) or hypoxic environment (2% oxygen) for a week before performing live-cell delivery assays. Both 20 and 2% oxygen cultured cells were maintained at the same passage number throughout the experiments. Absence of *Mycoplasma* contamination of cells was confirmed using the PCR Mycoplasma Test Kit II (PromoKine).

Experimental treatments described below (*e.g.* washing steps, addition of peptide) were performed in a biosafety cabinet under ambient oxygen (20% O_2). However, to minimize exposure to oxygen, media and solutions used for hypoxic conditions were degassed with 2% O_2. In addition, subsequent incubations (*e.g.* 1 h with peptide) were performed in the 2% oxygen chamber. All experiments presented were performed in triplicate, *i.e.* on different days and using different cell batches (cells were, however, passaged an identical number of times from a common stock).

Live-cell Delivery and Imaging—All cell delivery experiments were performed by seeding cells in 8-well chambered glass plate (Nunc) for 24 h to reach 80–90% confluency. Each well was washed three times with Dulbecco's phosphate-buffered saline (PBS) (HyClone) and Leibovitz medium (HyClone). Cells were incubated with 1–10 μM peptide in L-15 medium (not supplemented with serum) for 1–60 min at 37 °C (peptide concentration and incubation time were dependent on the condition of each experiment). Cells were then washed three times with L-15 medium supplemented with heparin (1 mg/ml, Sigma) to remove extracellular peptide. The cells were stained with 5 μM SYTOX Blue (Life Technologies, Inc.) to monitor cell viability during fluorescence microscopy imaging. All images were captured by an inverted epifluorescence microscope (Model IX81, Olympus) equipped with a Rolera-MGI Plus back-illuminated electron-multiplying charge-coupled device camera (QImaging). Images were acquired using phase contrast and three standard fluorescence filter sets as follows: cyan fluorescent protein (excitation (Ex) = 436 ± 10 nm/emission (Em) = 480 ± 20 nm), RFP (Ex = 560 ± 20 nm/Em = 630 ± 35 nm), and FITC (Ex = 488 ± 10 nm/Em = 520 ± 20 nm). The fluorescence intensities of cells were analyzed with SlideBook 4.2 software (Olympus).

Cell Viability and Proliferation Assays—To monitor the permeability of the plasma membrane, cells were incubated with cell-impermeable nucleic acid-staining SYTOX Blue dye (Life Technologies, Inc.) after peptide delivery or oxidant challenge. The proliferation of cells was examined using 3-(4,5-dimethylthiazol-2-yl)-2,5-diphenyltetrazolium bromide assay (Molecular Probes) following the manufacturer's instructions. In short, cells were cultured in 6-well plates to 80–90% confluency and treated with oxidants (50 μM for 30 min) or TMR-r13 (1 μM for 1 h) at 37 °C. Cells were then washed with PBS three times and detached by 0.5% trypsin solution. Trypsinized cells were resuspended in DMEM supplemented with 10% FBS and 1× penicillin/streptomycin. Cell solution was transferred to 96-well plates with 100 μl in each well. After culturing for 12 h, the cell proliferation rate was determined at specific time points. Cell proliferation was measured by removing DMEM in the well followed by adding 100 μl of fresh DMEM and 10 μl of 12 mM 3-(4,5-dimethylthiazol-2-yl)-2,5-diphenyltetrazolium bromide solution. The 96-well plate was incubated at 37 °C for 4 h. Each well was then mixed thoroughly with 100 μl of 10 mM SDS-HCl solution and incubated at 37 °C for 12 h. The formation of formazan catalyzed by cell mitochondrial reductase was measured by spectrometry at 560 nm. In parallel, cells incubated with vehicle (either PBS+ or L-15 medium, depending on the reagent tested) served as controls. PBS+ is PBS solution supplemented with calcium (100 mg/L) and magnesium (100 mg/L) (HyClone).

Cell Penetration Mechanism Assays—To inhibit endocytic processes, cells were first washed with warm PBS three times and pre-treated with 50 μM amiloride (Sigma) or 200 nM bafilomycin A1 (Sigma) for 20 min. Alternatively, cells were washed with cold PBS and pre-incubated at 4 °C for 30 min. Then cells were incubated with 1 μM TMR-r13 peptide in the presence of the same concentration of inhibitor (50 μM amiloride or 200 nM bafilomycin A1) for 60 min at 37 °C or at 4 °C with TMR-r13 peptide alone for 60 min. In contrast, cells were pre-loaded with

peptide cargos in late endosomes/lysosomes by incubating with 20 μM DEAC-k5 in L-15 medium for 1 h at 37 °C. Extracellular DEAC-k5 was removed by washing cells with heparin (1 mg/mL) solution and L-15 medium three times. The DEAC-k5-loaded cells were then incubated with 5 μM TMR-r13 in L-15 medium for 1 h at 37 °C. The cytosolic penetration efficiency of TMR-r13 and DEAC-k5 was evaluated by the method described above. The peptide cargo-loaded cells treated with 5 μM dfTAT peptide in L-15 medium without cystine for 1 h at 37 °C were used as a positive control.

To illustrate the accumulation of peptide in endocytic vesicles, cells were incubated with TMR-r13 (3 μM) or DEAC-k5 (20 μM) for 1 h. Extracellular peptides were removed by heparin solution (1 mg/ml) and L-15 medium wash three times. LysoTracker Green (500 nM, Molecular Probes) was added to cells for 30 min. Cells were washed with L-15 medium three times before imaging.

Cell Redox Treatments—Cells were pre-oxidized with various concentrations of freshly prepared pro-oxidants (cumene-OOH or H_2O_2) in PBS+ for 30 min at 37 °C. In contrast, to reduce cellular oxidative stress, cells were cultured in low glucose DMEM supplemented with various antioxidants, including 1 mM pyruvate (HyClone) (37), 250 μM α-tocopherol (Sigma) (38), 250 μM Trolox (Sigma), 75 μM ascorbic acid (MP Biomedicals) (39), 500 μM 2-phospho-L-ascorbic acid (Sigma) (39), and 100 nM sodium selenite (Mallinckrodt Pharmaceuticals) (40) for 48 h. Medium containing freshly prepared antioxidants was added every 24 h.

To feed cells with oxidized lipids, a lipid suspension was prepared. PGPC or PazePC (Avanti Polar Lipids) stock solution in chloroform was dried under a nitrogen stream to obtain a lipid film. The film was placed in a desiccator under vacuum overnight to eliminate the trace of solvent. The dry lipid film was resuspended in PBS+ by sonication for 10 min. The PGPC or PazePC (37.5 μM) solution was added to cells and incubated for 15 min at 37 °C. Cells were washed with heparin (1 mg/mL) solution and L-15 medium three times, followed by incubating with 1 μM TMR-r13 for 10 min at 37 °C.

Membrane Oxidation Detection—The C11-BODIPY$^{581/591}$ probe (Life Technologies, Inc.) purchased from the vendor was resuspended in pure ethanol to create a stock solution. The probe was diluted in L-15 medium to 15 μM and was incubated with cells for 30 min at 37 °C. Unincorporated probe was removed by washing cells with PBS and L-15 medium three times. Cellular oxidized C11-BODIPY$^{581/591}$ signal was detected by microscopy using a FITC filter set (Ex = 488 ± 10 nm/Em = 520 ± 20 nm), followed by quantitative analysis utilizing flow cytometry. Cells were detached by trypsinization and resuspended in L-15 medium. Signal of oxidized probe was examined by a flow cytometer (BD Accuri C6 model) installed with standard detector FL1 (Ex = 488 nm/Em = 533 ± 30 nm) and FL2 (Ex = 488 nm/Em = 585 ± 40 nm). All data were acquired at flow rate of 66 μl/min with a minimum of 20,000 events. The obtained signal was analyzed statistically using Flowjo version 10 software. Alternatively, the stock solution of DPPP (Life Technologies, Inc.) was prepared by dissolving in DMSO under a nitrogen atmosphere and was stored at −20 °C. HDF or MCH58 cells cultured in a 60-mm culture dish were detached by 0.5% trypsin solution. The cell solution was incubated with 100 μM DPPP for 5 min and was transferred to a 96-well plate. The fluorescence intensity of the oxidized DPPP probe was measured by GloMax-Multi Microplate Multimode Reader (Promega) equipped with UV optical kit (Ex = 365 nm/Em = 435 ± 25 nm). The oxidized DPPP signal was normalized by cell numbers counted by a flow cytometer (BD Accuri C6 model). The samples without adding DPPP or cells serve as negative controls.

Anti-Ox-PC Antibody Treatment—E06 mAb (Avanti Polar Lipids) was diluted in L-15 medium to a final concentration of 50 μg/ml and incubated with cells for 2 h at 37 °C. After washing antibody-treated cells with PBS and L-15 medium three times, 1 μM TMR-r13 in L-15 medium was added to the cells for 10 min at 37 °C. Heparin (1 mg/ml, Sigma) in L-15 medium wash was then applied three times to remove excess and membrane-bound peptide. Cell images were recorded as described above. The anti-AGE mouse IgM κ (ab18400, Abcam), the same isotype with E06 mAb, served as a negative control (41). To inactivate E06 mAb, 20 μg/ml phosphorylcholine salt (Fisher) was pre-mixed with antibody in L-15 medium before incubating with the cells.

Partitioning Assay—The experiment was performed following the procedures reported by Sakai and Matile (42). In short, anhydrous DOPC (Avanti Polar Lipids) lipid film was prepared and was resuspended in hexane by sonication. In contrast, PGPC or PazePC was dissolved in 1-octanol (Sigma) and was mixed with DOPC solution to a molar ratio of 1:9 (PGPC/DOPC or PazePC/DOPC). The partitioning was performed by an adding equal volume of 3 mM lipid solution and 5 μM peptide in PBS (pH 7) in a microcentrifuge tube and mixing vigorously. The fluorescence signal of peptide in either the organic or aqueous phase was quantified by GloMax-Multi Microplate Multimode Reader (Promega) with Green Optical Kit (Ex = 525 nm/Em = 610 ± 30 nm).

Statistical Analysis—All statistical analyses were performed using paired two sample for means *t* test.

Results

Identification of Efficient CPPs and Robust Cytosolic Penetration Assay—Given the seemingly capricious nature of cytosolic penetration, our first objective was to identify a compound that would penetrate cells efficiently so as to have a robust assay for measuring cytosolic penetration quantitatively. Following the work of Futaki and co-workers (15, 18), Brock and co-workers (16), among others (17), we first tested the cytosolic penetration of linear polyarginine peptides containing an increasing number of arginine residues (from 5 to 13) and labeled with TMR by fluorescence microscopy. Peptides were synthesized with all L- or all D-amino acids (named as L-CPPs or D-CPPs, respectively). The peptides containing 7 amino acids or less showed no apparent cytosolic penetration in human skin fibroblasts (HDF and immortalized skin fibroblasts, MCH58). In contrast, the peptide with 9 arginine residues displayed cytosolic penetration in MCH58 but not in HDF. Finally, peptides with 11 or 13 residues displayed significant levels of cytosolic penetration in both cell types (Fig. 1*A*). Penetration was established by observing nucleolar staining by the peptides at high magnification (×100) (Fig.

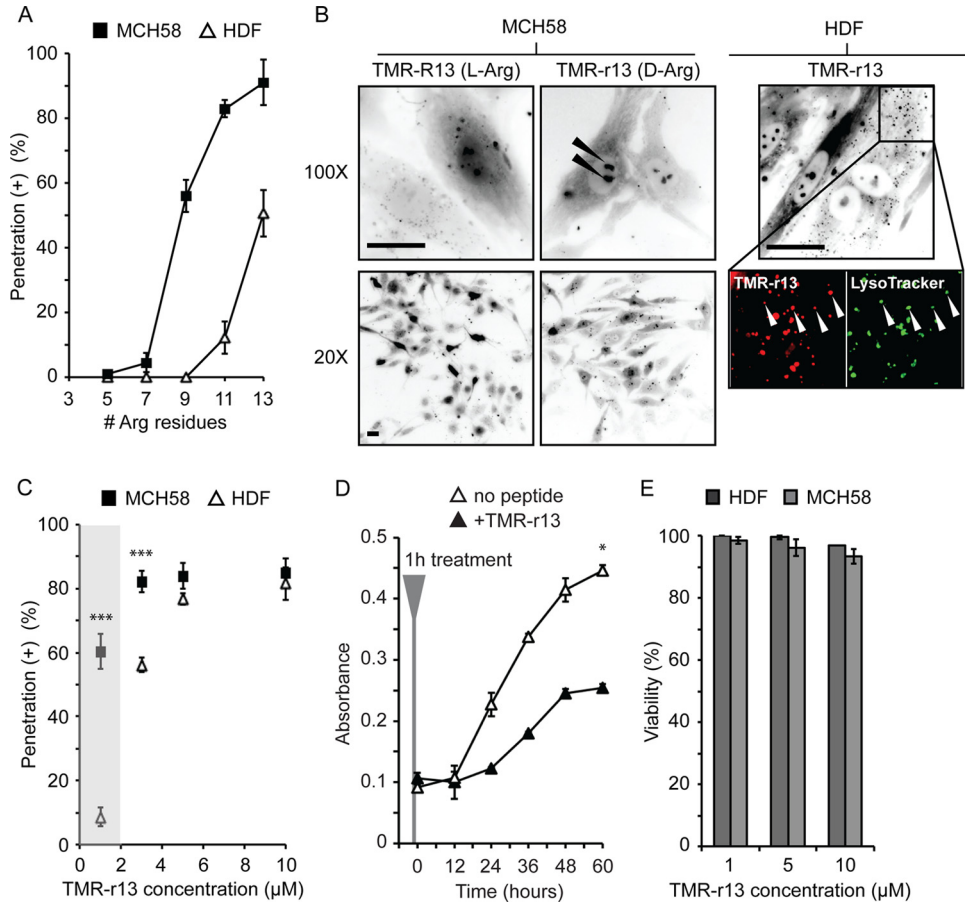

FIGURE 1. **Identification of polyarginine CPPs with high cytosolic delivery efficiencies.** *A,* delivery efficiencies of polyarginine peptides in HDF and MCH58 cells (TMR-Rn, $n = 5–13$, 3 μM, 1-h incubation). *B,* representative images of MCH58 cells incubated with TMR-R13 or TMR-r13 (5 μM, 1 h). Nucleolar staining can be seen with TMR-R13 at ×100 magnification. However, this staining is less pronounced upon ×20 imaging. In contrast, nucleolar staining is visible with TMR-r13 using both ×100 and ×20 imaging (highlighted by *arrows*). In HDF, a cell type less prone to cell penetration than MCH58, TMR-r13 (3 μM, 1 h) also shows a punctate distribution. Zoomed-in images show co-localization of puncta (highlighted by *arrows*) containing TMR-r13 (pseudocolored *red*) and LysoTracker (pseudocolored *green*), suggesting entrapment of TMR-r13 in acidic endocytic organelles. In all images, cells were resistant to staining by SYTOX Blue, indicating that their plasma membrane was not compromised. Images are inverted monochromes of TMR fluorescence emission (RFP filter). *Scale bars,* 20 μm. *C,* dose dependence of the cytosolic penetration of TMR-r13. The efficiency of cytosolic penetration was measured in MCH58 and HDF cells as the percentage of cells positive for nucleolar peptide staining and negative for SYTOX Blue staining. The region marked in *gray* highlights how MCH58 cells are significantly more prone to cellular penetration than HDF at 1 μM TMR-r13. *** represents $p \leq 0.001$ compared with HDF at same peptide concentration. *D,* proliferation rate of HDF cells treated with TMR-r13 (5 μM, 1 h) is reduced when compared with untreated cells. * represents $p \leq 0.05$ compared with untreated cells. *E,* treatment of HDF cells with TMR-r13 (1, 5, and 10 μM) for 1 h did not reduce cell viability, as measured by SYTOX Blue exclusion assay. Similar results were obtained for MCH58 cells. The data in *A, C, D,* and *E* represent the mean of triplicate experiments and the corresponding standard deviations.

1*B*). This staining is common for arginine-rich peptides, and because cytosolic entry presumably precedes nucleolar staining, it indicates that CPPs reach the intracellular cytosolic/nuclear milieu (15–18). Importantly, this specific staining was observable at ×20 magnification for D-CPPs but not for L-CPPs (Fig. 1*B*). This is presumably because, unlike the protease-resistant D-CPPs, L-CPPs degrade rapidly inside cells. Consequently, the fluorescence associated with L-CPPs was more diffuse overall, and nucleolar staining was not clearly detectable at a low magnification. In turn, the cytosolic/nucleolar signal could not be convincingly distinguished from unrelated signals (peptide inside endosomes, peptide bound to cell surface, etc.) at low magnification, making quantification of the penetration of L-CPPs problematic and unconvincing. In contrast, quantification of cell penetration was straightforward with D-CPPs as these reagents led to unequivocal nucleolar/cytosolic staining at a magnification compatible with the surveying of a large number of cells. We therefore focused on this class of reagent for the rest of the study and used a penetration assay that relies on simply counting the number of cells that show nucleolar staining in a culture after incubation with peptide. In this assay, dead cells are identified by staining with the dye SYTOX Blue. Overall, cells displaying nucleolar staining and excluding SYTOX Blue are considered positive for peptide cytosolic penetration (presented as % penetration (+) in figures.).

As the most active compound in the series, TMR-r13, where r is the one-letter code for D-Arg, was characterized in greater detail. The dose-dependence of TMR-r13 on penetration showed that the peptide penetrates both MCH58 and HDF cells equally efficiently at 5 μM or above (Fig. 1*C*). At lower concentrations, MCH58 cells are, however, more prone to penetration than HDF. Notably, cells examined were resistant to staining with SYTOX Blue and were viable and proliferating up to 60 h after incubation with the peptide (Fig. 1, *D* and *E*). The rate of proliferation of cells treated with TMR-r13 was markedly slower than untreated cells, a phenomenon we attribute to the

prolonged retention of the protease-resistant CPP inside cells.[3] Overall, TMR-r13 nonetheless displays a cytosolic penetration activity that is high, easily quantifiable, and non-toxic at the concentrations tested.

TMR-r13 Translocates across the Plasma Membrane—In cells without a strong cytosolic/nucleolar signal, TMR-r13 can be seen trapped inside endosomes (Fig. 1*B*), indicating that TMR-r13 is capable of endocytosis. This mode of entry is common for arginine-rich CPPs as these compounds are often internalized by macropinocytosis (19). This then raises the question of whether endocytosis is a required step preceding cytosolic entry or whether it is a process occurring in parallel to an endocytosis-independent penetration mechanism. To address this, we first tested the effect of amiloride and bafilomycin, inhibitors of macropinocytosis and endosomal acidification, respectively, on cellular entry. These inhibitors did not decrease the cytosolic penetration activity of TMR-r13. Similarly, incubation of TMR-r13 with cells was performed at 4 °C, a condition that inhibits energy-dependent endocytic uptake. This low temperature condition only led to a minor reduction in cell penetration (Fig. 2*A*) (15, 17, 18). In addition, cytosolic penetration was achieved in a relatively high percentage of cells within 1 or 3 min of incubation, making a process involving endocytosis and endosomal escape upon slow endocytic maturation unlikely (typical time frame varies from 5 to 30 min) (Fig. 2*B*) (43). Furthermore, TMR-r13 did not cause the release of fluorescent material pre-loaded within endosomes. In contrast, the positive control, dfTAT, an endosomolytic reagent, efficiently induced the endosomal escape of endocytosed material (Fig. 2*C*) (20). This suggests that cytosolic penetration of TMR-r13 does not involve leakage from the endocytic pathway. Overall, these data indicate that the peptide does not require endocytosis to gain access to the cytosol. In turn, exclusion of this possibility indicates instead that the peptide enters the cytosolic space by crossing the plasma membrane directly. To test whether the plasma membrane translocation of the peptide enhanced the permeation of other molecules, TMR-r13 was co-incubated with fluorescent molecules of various sizes, including the small molecule SYTOX Green and fluorescently labeled peptides. Although TMR-r13 entered cells in all assays, no other fluorescent material could be detected within the cells, indicating that the TMR-r13-mediated translocation was not accompanied by transient membrane leakage (Fig. 2*D*).

Reduced Oxidative Stress Decreases Cytosolic Penetration—The previous experiments were carried out with cells exposed to 20% oxygen during culture (ambient air supplemented with 5% carbon dioxide, standard protocols). If oxidation affects transport across membranes as originally postulated, one would expect that reducing oxidative stress should decrease cytosolic penetration. To test this, MCH58 cells were grown for a week at either 20% oxygen or in a sealed chamber flushed with 2% oxygen, 5% carbon dioxide, and 93% nitrogen. MCH58 cells were chosen for this assay because they appear more prone to cell penetration than HDF and therefore provide a cell line more adequate for inhibition studies (Fig. 1*C*). Cells were then exposed to TMR-r13 (1 μM) for 1 h, and the number of cells positively displaying nucleolar staining was counted. Under these conditions, hypoxia did not appear to impact the percentage of cells positive for cell penetration (Fig. 3*A*). However, a more careful examination of the process showed significant differences when incubation time with peptide was shorter (Fig. 3*B*). In addition, the overall amount of peptide entering cells, quantified by flow cytometry, was reduced when compared with 20% oxygen (Fig. 3*B*). This indicates that although cytosolic penetration is still possible at low oxygen levels, this process is partially inhibited, as less peptide is able to enter cells. Assuming that cytosolic penetration might still be permitted by oxidized species that remain present even at low oxygen tension, we next added an antioxidant mixture to the growth media to further reduce the oxidative stress experienced by cells. This mixture includes pyruvate, α-tocopherol, Trolox, ascorbic acid, 2-phospho-L-ascorbic acid, and sodium selenite. These species are either scavengers of oxidants or co-factors of enzymes that deplete cells from oxidized species (38–40, 45). The antioxidant mixture had a pronounced effect on reducing the percentage of cells positive for TMR-r13 and, in combination with 2% oxygen, almost abolished cytosolic penetration (Fig. 3*A*).

Because TMR-r13 is the most active compound tested in our polyarginine series, we next examined how hypoxia would impact a less potent peptide (Fig. 1*A*). For this assay, TMR-r9 was tested as nona-arginine CPPs are widely used as delivery agents (46–48). When using MCH58 cells grown at 20% oxygen, TMR-r9 required an incubation concentration of 1 μM to achieve a penetration efficiency equivalent to that obtained with TMR-r13 (~65% penetration of positive cells after 1 h of incubation). When these conditions were used with cells grown at 2% oxygen, the penetration of TMR-r9 was abolished (Fig. 3*C*). Overall, this indicates that the impact of hypoxia is increasingly more pronounced as the potency of the CPP is reduced. Inversely, this also suggests that oxidative processes are required for the penetration of CPPs.

Increasing Oxidation Enhances Cytosolic Penetration—If a reduction in oxygen tension decreases cell penetration, one would expect that increasing oxidative stress might conversely enhance cellular entry. To test this, cells were partially oxidized with oxidants, and the impact of these reagents on penetration was established. In these assays, we used HDF cells because of their lower propensity for polyarginine cytosolic penetration (Fig. 1*C*). Cells were treated with the lipophilic oxidant cumene hydroperoxide (cumene-OOH) or with hydrogen peroxide (H_2O_2). The concentration of oxidants was kept low in these experiments so as to not impact cell viability and proliferation (Fig. 4*A*, the similarity between the proliferation rates of treated *versus* untreated cells is used as an indication that cells remain relatively healthy after mild oxidation). Treatment with both cumene-OOH and H_2O_2 increased the cytosolic penetration efficiency of TMR-r13 (Fig. 4*B*). Cumene, a non-oxidant control compound, did not significantly impact TMR-r13 delivery, indicating that the lipid bilayer insertion of the cumene moiety of cumene-OOH is not significantly altering the permeability of the membrane. Treatment with cumene-OOH increased the cytosolic penetration efficiency of TMR-r13 and TMR-r11 and

[3] K. Najjar and J. P. Pellois, unpublished data.

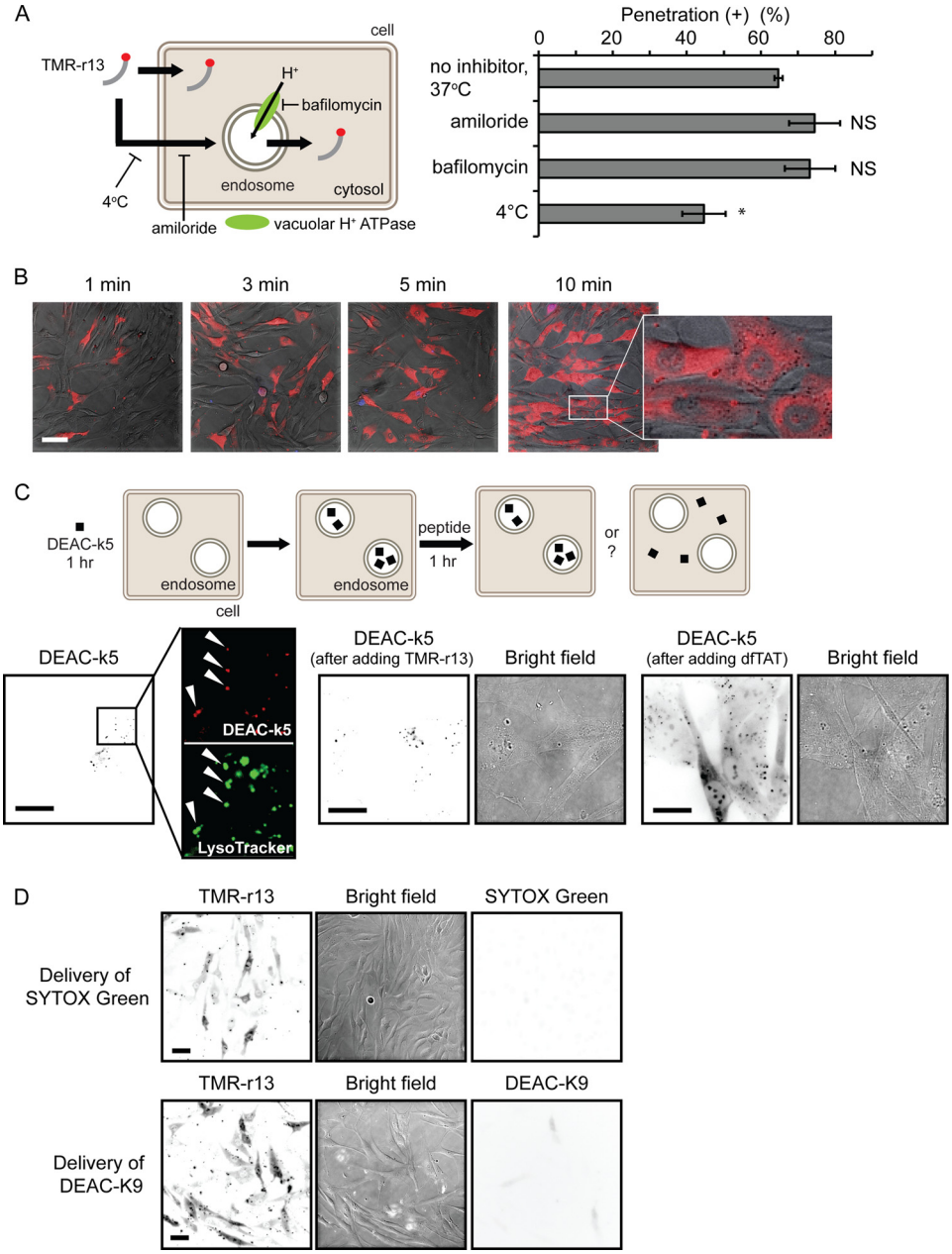

FIGURE 2. **TMR-r13 does not utilize the endocytic pathway to access the cytosolic space of cells.** *A,* inhibitors of endocytic processes do not prevent cytosolic penetration. MCH58 cells were pretreated with 50 μM amiloride, 200 nM bafilomycin, or PBS supplemented with calcium and magnesium (vehicle) for 20 min. Cells were then incubated with inhibitors and with TMR-r13 (1 μM) for 1 h. Alternatively, cells were maintained at 4 °C during peptide incubation. The data represent the means of triplicate experiments and the corresponding standard deviations. *NS* (not significant) represents $p > 0.05$, and * represents $p \leq 0.05$ compared with cells with no inhibitor at 37 °C. *B,* images of MCH58 cells treated with 5 μM TMR-r13 for the indicated times. Images are overlay of bright field, TMR-r13 (pseudocolored *red*), and SYTOX Blue (pseudocolored *blue*). A zoomed-in image shows distinct nucleolar staining of TMR-r13 without SYTOX Blue staining. *Scale bar,* 50 μm. *C,* TMR-r13 (5 μM, 1 h) fails to release DEAC-k5 from endocytic pathway when the endosomolytic agent dfTAT does. HDF cells were pre-incubated with DEAC-k5 (20 μM, 1 h, k is the one-letter code for D-lysine). Accumulation of DEAC-k5 (pseudocolored *red*) within endocytic organelles is established by co-localization with LysoTracker (pseudocolo*red green*) (highlighted by *arrows*). Cells were then treated with TMR-r13 or dfTAT and imaged. Images are inverted monochromes of fluorescence emission and monochromes of bright field imaging. *Scale bars,* 50 μm. *D,* membrane translocation by TMR-r13 is not accompanied by penetration of the small molecule SYTOX Green or the peptide DEAC-K9. Cells were incubated for 1 h at 37 °C with both TMR-r13 (1 μM) and SYTOX Green (5 μM), a green cell-impermeable nuclear staining dye that can enter cells upon permeation of the plasma membrane. After peptide delivery, cells were washed and incubated with SYTOX Blue, a nuclear stain similar to SYTOX Green but with extinct excitation wavelength. TMR-r13 penetrated cells while excluding both SYTOX Green and SYTOX Blue. Similar results were obtained when SYTOX Green was substituted for DEAC-K9 (an oligolysine peptide labeled with the blue fluorophore DEAC). Fluorescence images are represented as inverted monochrome. *Scale bars,* 20 μm.

enabled cytosolic penetration by TMR-r9 at detectable levels (Fig. 4*C*). Peptides such as TMR-R7 or DEAC-K9 did not penetrate these cells, indicating that cells are not simply more permeable to all compounds (data not shown).

Membrane Oxidation Correlates with Cell Penetration—Oxidative stress can result in a broad spectrum of effects. Given that TMR-r13 appears to cross the plasma membrane of cells directly, we next chose to determine whether membrane oxidation correlates with the efficiency with which the peptide penetrates cells. First, we examined whether the conditions used in the previous oxidation experiments led to changes in membrane chemistry. The lipophilic reporter C11-BODIPY$^{581/591}$,

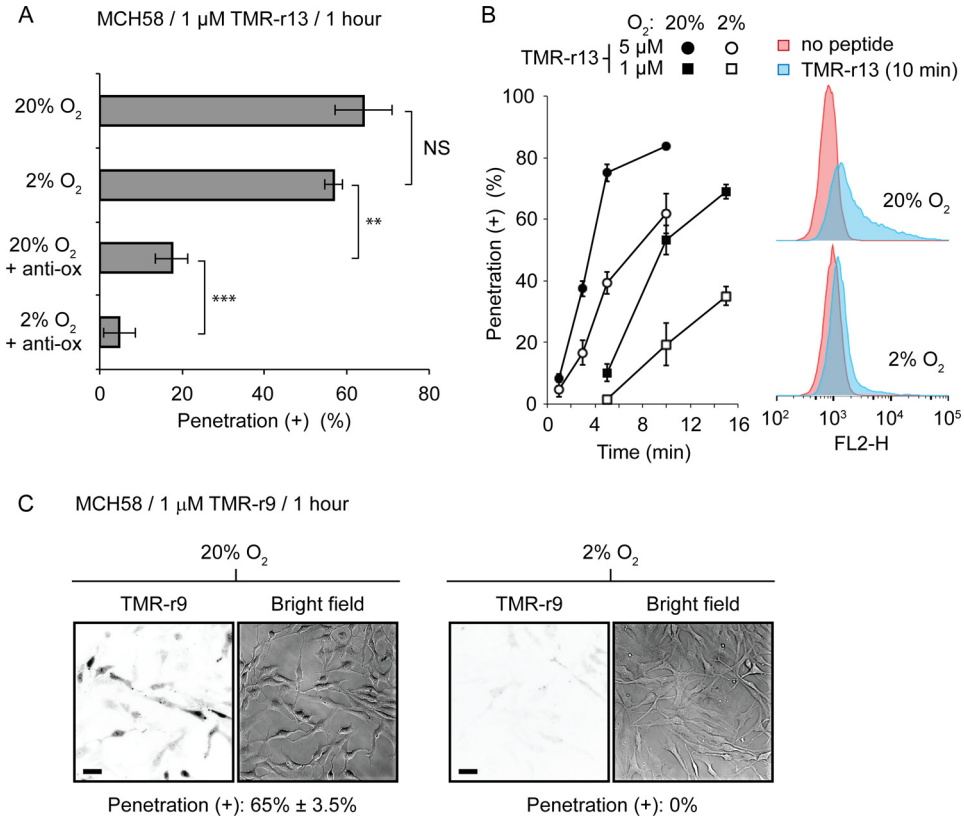

FIGURE 3. **Conditions of reduced oxidation decrease cytosolic penetration of TMR-r13.** *A,* MCH58 cells were grown under atmospheric (20% oxygen) or hypoxic (2% oxygen) conditions, in the presence or absence of a mixture of antioxidants. Cells were then treated with 1 μM TRM-r13 for 1 h. The vehicle is PBS supplemented with calcium and magnesium. *Anti-ox* corresponds to the antioxidant mixture. *NS* represents $p > 0.05$; ** represents $p \leq 0.01$, and *** represents $p \leq 0.001$. *B,* cytosolic penetration of TMR-r13 (1 μM) is slower in cells grown at 2% than 20% oxygen. Hypoxia also reduces the amount of peptide-penetrating cells, as shown by flow cytometry. FL2-H is signal intensity of sample in the FL2 channel (Ex = 488 nm/Em = 585 ± 40 nm, used for detection of TMR-r13). *C,* cytosolic penetration of TMR-r9 (1 μM, 1 h) is abolished in MCH58 cells cultured at 2% oxygen. Images are inverted monochromes of TMR fluorescence emission (RFP filter) and monochromes of bright field imaging. *Scale bars,* 20 μm. The data in *A* and *B* represent the means of triplicate experiments and the corresponding standard deviations.

was used to quantify the oxidation state of cellular membranes. The fluorescence emission of C11-BODIPY$^{581/591}$ changes from red (595 nm) to green (520 nm) upon oxidation (49). The susceptibility of C11-BODIPY$^{581/591}$ to oxidation is equivalent to that of endogenous polyunsaturated lipids present in cell membranes, and a change in fluorescence of this reporter can be used to infer overall lipid oxidation. An increase in green fluorescence was observed by both microscopy and flow cytometry when cells grown at 20% oxygen were treated with an increasing amount of cumene-OOH (no increase is observed with the control compound cumene). This indicates that cellular membranes are oxidized by the lipophilic oxidant (Fig. 5*A*). Notably, the cytosolic penetration of TMR-r13 correlated positively with the green fluorescence of C11-BODIPY$^{581/591}$ (Fig. 5*A*), supporting the notion that the oxidized membrane components might be involved in membrane translocation.

Because MCH58 cells are more prone to cell penetration than HDF cells, we next examined whether the difference in response between these two cell types could be accounted for by a difference in overall level of membrane oxidation. The previous C11-BODIPY$^{581/591}$ assay was not sufficiently sensitive to compare cells incubated at 20% oxygen (as shown in Fig. 5*A*, a weak C11-BODIPY$^{581/591}$ fluorescence signal is obtained when cumene-OOH is absent). To circumvent this problem, an assay using DPPP was performed instead. DPPP is a non-fluorescent lipophilic compound that reacts stoichiometrically with lipid hydroperoxides to yield a fluorescent DPPP oxide (50). MCH58 and HDF grown at 2 or 20% oxygen were incubated with DPPP, and the fluorescence of DPPP oxide obtained was quantified. The number of cells present in each sample was established by flow cytometry. Given that MCH58 and HDF have similar morphologies and sizes, the DPPP oxide fluorescence was then normalized to the total number of cells for comparison. As shown in Fig. 5*B*, the fluorescence of DPPP oxide was significantly greater in cells grown at 20% oxygen than in cells grown at 2% oxygen. In addition, MCH58 cells were also consistently more fluorescent than HDF, under similar growth conditions, indicating higher levels of lipid hydroperoxides in MCH58 than in HDF. Overall, these data indicate a positive correlation between membrane oxidation and cell penetration.

Involvement of Oxidized Lipids in Cell Penetration—As oxidants, cumene-OOH and H_2O_2 presumably generate a broad array of lipidic or proteinaceous membrane products. Similarly, the transition between 2 and 20% oxygen potentially leads to a variety of changes in cellular membrane composition. Identifying which membrane components impact translocation, directly or indirectly, might therefore be a challenging process. Based on the idea that oxidized lipids might bind TMR-r13 and participate in its translocation across a lipid bilayer, we next examined whether molecules that interfere with oxidized lipids

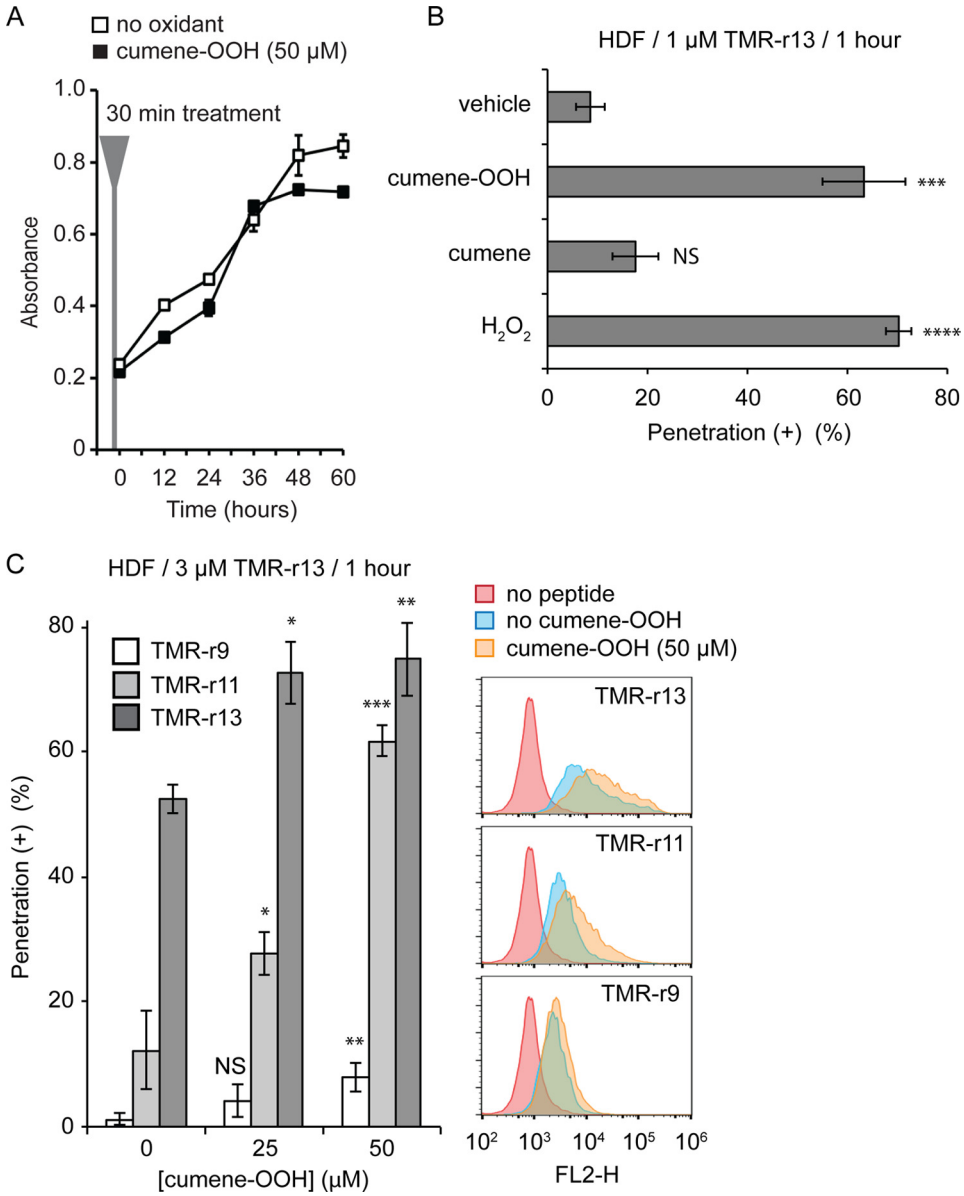

FIGURE 4. **Oxidants increase the cytosolic penetration of TMR-r13.** *A,* HDF cells treated with cumene-OOH (50 μM, 30 min) display a proliferation rate similar to untreated cells. *B,* cell penetration activity of TMR-r13 in HDF increases significantly in the presence of oxidants. HDF cells were pretreated with cumene-OOH, cumene, or H_2O_2 for 30 min and incubated with 1 μM TMR-r13 for 1 h. *** represents $p \leq 0.001$; **** represents $p \leq 0.0001$, and *NS* represents $p > 0.05$ compared with vehicle (PBS). *C,* cumene-OOH (0, 25, or 50 μM, 30 min) increases the activity of TMR-r13, TMR-r11, and TMR-r9 (3 μM, 1 h) in a dose-dependent manner in HDF cells. Cytosolic penetration was quantified by fluorescence microscopy (histogram) and flow cytometry. *NS* represents $p > 0.05$; * represents $p \leq 0.05$; ** represents $p \leq 0.01$, and *** represents $p \leq 0.001$ compared with cells not treated with cumene-OOH. FL2-H is signal intensity of sample in the FL2 channel (Ex = 488 nm/Em = 585 ± 40 nm, used for detection of TMR-r13). The data in *A–C* represent the mean of triplicate experiments and the corresponding standard deviations.

on the cell surface might inhibit cytosolic penetration. To this effect, the E06 monoclonal antibody (E06 mAb) was used. E06 mAb binds several by-products of the oxidation of phosphatidylcholine, often referred to as Ox-PC (51). Because phosphatidylcholine is a major component of the outer leaflet of the plasma membrane, it seemed reasonable that this antibody might be sufficient to display an effect (52). Cells were pretreated with E06 mAb (50 μg/ml) or a control IgM monoclonal antibody not targeting oxidized lipids (its epitope are advanced glycation end products) (41). The phosphorylcholine salt (PC salt) was also optionally added to media, as this molecule inhibits the binding of E06 mAb to the polar head of Ox-PC (53). IgM and the combination of E06 mAb/PC salt did not impact the cytosolic penetration activity of TMR-r13 (Fig. 6*A*). In contrast, E06 mAb caused a severe reduction in cytosolic penetration, suggesting that Ox-PC may be directly or indirectly mediating the activity of TMR-r13.

To test the plausibility of oxidized membrane components mediating peptide cytosolic entry, we chose to establish whether certain oxidized lipids could facilitate peptide translocation. For this assay, we chose PGPC and PazePC, oxidized products of PC (54). PGPC and PazePC are found in human tissue and are obtained upon oxidation of an unsaturated fatty acyl chain of PC, an abundant component of the plasma membrane of human cells (54). PGPC and PazePC were first preincubated with HDF cells. Cells were then washed to remove

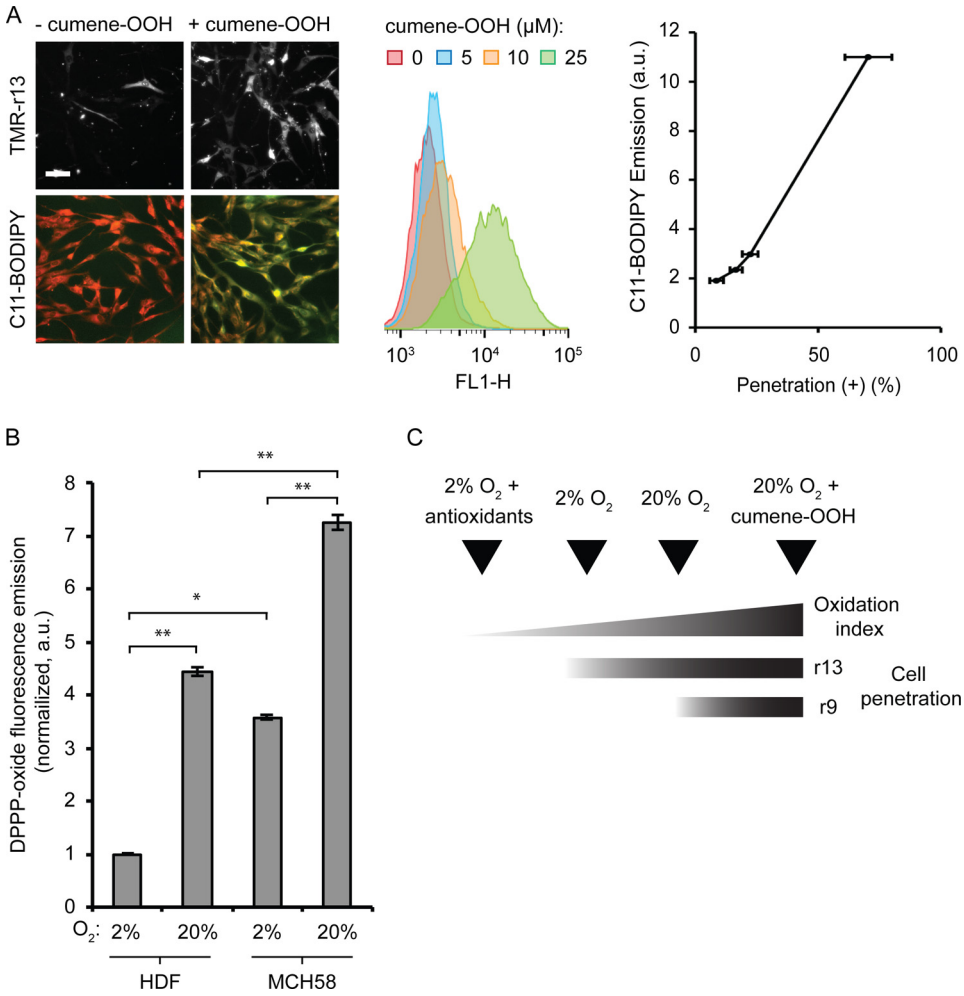

FIGURE 5. **Membrane oxidation and cytosolic penetration are positively correlated.** *A,* HDF cells were treated with cumene-OOH at various concentrations for 30 min. The cytosolic penetration efficiency of TMR-r13 (1 μM, 1 h) was measured. Images of TMR-r13 delivery are monochromes of TMR fluorescence emission (RFP filter). In parallel, membrane oxidation after cumene-OOH treatment was measured by flow cytometry using the green fluorescence of the lipophilic oxidation reporter C11-BODIPY$^{581/591}$. *FL1-H* corresponds to the signal intensity of sample in the FL1 channel (Ex = 488 nm/Em = 533 ± 30 nm, used for detection of the green fluorescence of C11-BODIPY$^{581/591}$). The correlation between the geometric mean of the C11-BODIPY$^{581/591}$ emission and the cytosolic penetration efficiency is reported. *Scale bar,* 20 μm. *B,* comparison of the levels of lipid peroxides in the membrane of HDF and MCH58 cells using the lipophilic DPPP probe. The fluorescence of oxidized DPPP present in cellular membranes of cells grown at 2% or 20% oxygen is reported as normalized to the total number of cells per sample and to the least oxidized sample (2%, HDF). * represents $p \leq 0.05$, and ** represents $p \leq 0.01$. *C,* scheme illustrating the relationship between the cellular penetration of TMR-r13 and TMR-r9 with membrane oxidation index.

extracellular unincorporated lipids, and the penetration activity of TMR-r13 was subsequently tested. The peptide, incubated with cells at 1 μM for 10 min, displayed poor penetration in cells treated with vehicle alone (PBS+ only, no oxidized lipids added) (Fig. 6*B*). In contrast, cells treated with PGPC and PazePC showed a significantly higher susceptibility for peptide penetration (Fig. 6*B*).

To test whether PGPC and PazePC might promote cell penetration by directly interacting with TMR-r13, we examined how these lipids impact the partitioning of the peptide between PBS and hexane. In this assay, hexane is used to mimic the environment of low dielectric constant of the lipid bilayer, and partitioning is used as a measure of how hydrophobic or hydrophilic a substance is. As shown in Fig. 6*C*, TMR-r13 is present in the aqueous phase, by itself or when incubated with DOPC. In contrast, addition of PGPC or PazePC (9:1 non-oxidized/oxidized lipid) promotes the transfer of the peptide into the hydrophobic environment. These results therefore establish that the oxidized lipids PGPC and PazePC can interact with TMR-r13 and change the properties of the peptide in respect to partitioning between an aqueous environment and that of low dielectric constant. Overall, these results establish that these oxidized species can enhance the cytosolic penetration activity of TMR-r13 and that, given the partitioning results obtained, the lipids mediate this effect by directly interacting with TMR-r13.

Discussion

Our results establish that the conditions used during cell growth markedly impact the permeability of cells for polyarginine CPPs. Under all conditions tested, the oxidation index (or how oxidizing the growth conditions are) positively correlates with how efficiently the CPPs tested enter the cytosol of cells (Fig. 5*C*). Given that the translocation of the peptides appears to take place at the plasma membrane, it is reasonable to postulate that oxidation alters the properties of this membrane and that certain oxidized membrane components mediate or facilitate

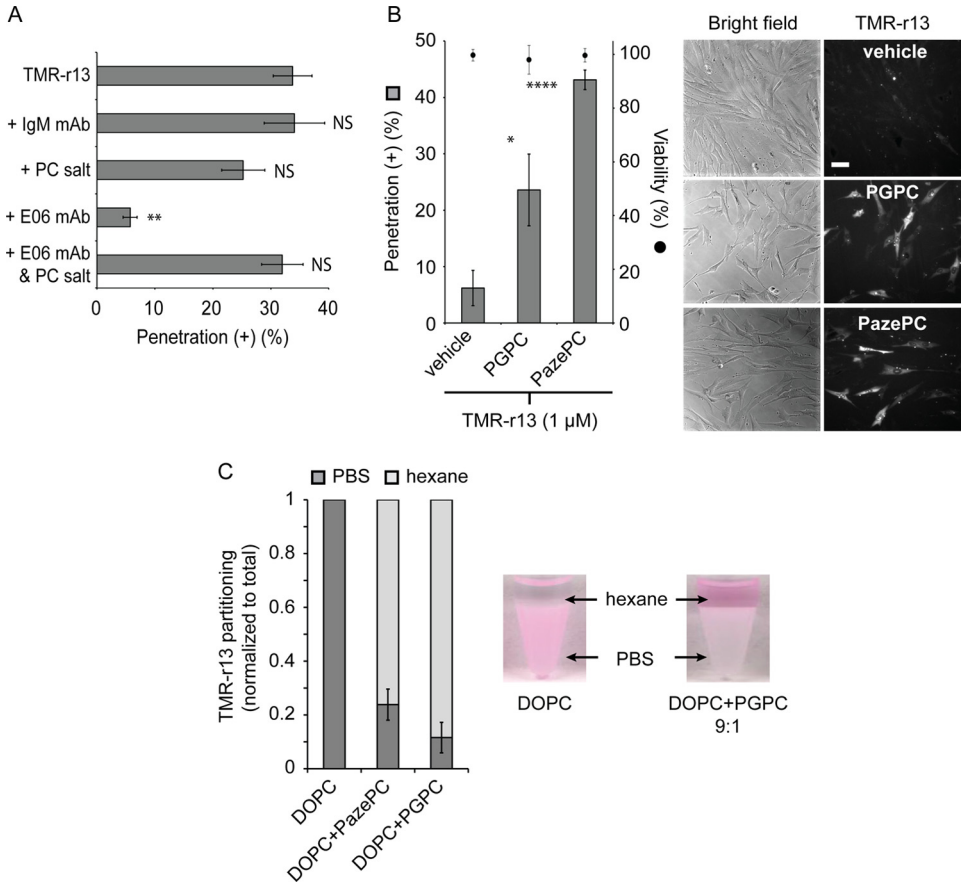

FIGURE 6. **Oxidized lipids are capable of mediating the membrane translocation of TMR-r13.** *A,* E06 mAb inhibits cytosolic penetration of TMR-r13. MCH58 cells were pretreated with IgM (50 μg/ml), phosphorylcholine salt (20 μg/ml), E06 mAb (50 μg/ml), or E06 mAb and PC salt. Cells were then treated with TMR-r13 (1 μM, 10 min), and the cytosolic penetration of the peptide was quantified. *NS* represents $p > 0.05$, and ** represents $p \leq 0.01$ compared with cells treated with TMR-r13 alone. *B,* oxidized lipids PGPC and PazePC promote the cytosolic penetration of TMR-r13. HDF cells were pretreated with the lipids, washed, and incubated with peptide (1 μM, 10 min). Vehicle is PBS. * represents $p \leq 0.05$, and **** represents $p \leq 0.0001$ compared with vehicle (PBS). Cell viability was measured using SYTOX Blue exclusion after TMR-r13 delivery. Representative bright field images and monochrome images of TMR fluorescence emission (RFP filter) are shown. *Scale bar,* 20 μm. *C,* anionic lipids mediate the transfer of TMR-r13 from an aqueous phase to a milieu of low dielectric constants. TMR-r13 (5 μM) was dissolved in PBS (pH 7), and an equal volume of hexane containing the lipids listed (3 mM) was added. The amount of peptide equilibrating between each phase after mixing was quantified by fluorescence spectroscopy. The *graph* displayed represents the relative fraction of peptide present in the aqueous and organic phases. DOPC was mixed with the oxidized lipids PGPC or PazePC at a ratio of 9:1. The data in *A–C* represent the mean of triplicate experiments and the corresponding standard deviations.

this process. Differences in oxidative damage or, inversely, how cells repair oxidative damage could explain variability in CPP performance from cell to cell, from cell type to cell type, or between various experimental conditions (*e.g.* media with or without antioxidants).

An important question is whether membrane oxidation is necessary for cytosolic penetration or merely facilitates it. Anaerobic conditions are lethal to human cells and suppression of oxidative stress by complete removal of oxygen is therefore not testable. In contrast, cells thrive at 2% oxygen (55, 56). This cell growth condition was however not sufficient to abolish cytosolic penetration. In addition, the presence of lipid peroxides was detected in cellular membranes under these conditions, indicating that some level of membrane oxidationo persists even at low oxygen tension. Notably, addition of antioxidants showed a more pronounced inhibitory effect, presumably by further diminishing the number of oxidized species present at the plasma membrane. This would then support the notion that oxidized species are required to achieve translocation. In addition, comparison between TMR-r13 and shorter oligoarginine peptides suggests that TMR-r13 represents a highly active member within a large family of CPPs. If oxidation is critical in mediating the activity of TMR-r13, it should be even more so for less active compounds. Our data support this notion as hypoxia completely inhibited the cytosolic penetration of TMR-r9. We therefore conclude that membrane oxidation is required for cytosolic penetration by linear oligoarginine CPPs at low micromolar concentrations.

How membrane oxidation mediates peptide penetration on a molecular level remains currently unclear. It is possible that membrane oxidation changes the general properties of the plasma membrane and that peptide translocation does not directly involve oxidized species. For instance, membrane oxidation can alter membrane fluidity, and this alone could change the permeability of the cell (57, 58). In addition, Melikov *et al.* (59) have suggested that surface-exposed phosphatidylserine (PS) mediates the translocation of polyarginine peptides into cells. Interestingly, lipid bilayer oxidation has been shown to promote the flip-flop of PS, a lipid that is otherwise typically present on the inner leaflet of the plasma membrane (60). In

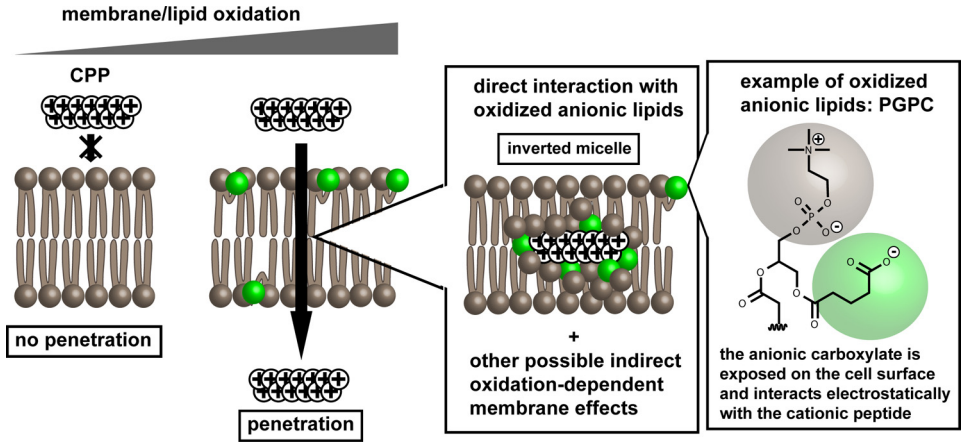

FIGURE 7. **Proposed model for the oxidation-dependent plasma membrane translocation of polyarginine peptides.** Under low oxidative stress conditions, cationic arginine-rich CPPs are unable to translocate across membranes efficiently. In contrast, membrane oxidation leads to the accumulation of oxidized lipids in the lipid bilayer. These oxidized lipids, including anionic oxidized phosphatidylcholine species (PGPC is represented as an example), interact with cationic arginine-rich CPPs on the cell surface. Inverted micelles comprising oxidized lipids are plausible structures that might mediate the translocation of CPPs across the bilayer. Other membrane oxidation effects, including changes in membrane fluidity and introduction of bilayer defects, are likely to also modulate the efficiency with which translocation occurs.

this context, membrane oxidation might contribute to an increase in the amount of PS present on the cell surface and thereby promote peptide translocation. Alternatively, oxidized species, including oxidized lipids, could be directly involved in interacting with polyarginine peptides and mediate their transport. Oxidation chemistry is, however, extremely complex and gives rise to a wide variety of products. For instance, simple exposure of a dry unsaturated phospholipid to air produces a wide spectrum of oxidized by-products (>20 species) (54). Non-enzymatic oxidation reactions also involve propagation steps that can dramatically amplify the effect of an initial oxidation event. This is the case for lipid peroxidation where the abstraction of a single hydrogen from a polyunsaturated fatty acid by reactive oxygen species initiates a cascade of oxidation reactions that can subsequently damage a large number of neighboring lipids within a membrane (61). Each lipid peroxide formed in this process can then decompose into a multitude of products. The cell counteracts this damage using a wide variety of mechanisms, ranging from protection with antioxidants to enzymatic repair or degradation (62). As a result of this complexity, the identity of oxidized lipids present in a membrane and their respective levels remain poorly characterized. This study, however, highlights that a thorough examination of how the composition of cellular membranes changes with oxidation is now required to shed light on the mechanisms of membrane translocation.

To gain mechanistic insights into oxidation-dependent cell penetration of TMR-r13, we decided to test whether pure and physiologically relevant oxidized lipids could modulate the activity of TMR-r13. Several reports have already highlighted that anionic amphiphiles can enhance the translocation of polyarginine peptides by acting as lipophilic counterions. Pyrene butyrate can, for instance, be used as an extracellular additive that can improve cell penetration of the CPPs R9 (63). Other anionic amphiphiles have displayed similar behavior (42). A mechanism of action proposed involves the formation of transient inverted micelles between the anionic compounds and the cationic peptides. We therefore envision that membrane oxidation could promote peptide translocation by mediating the formation of anionic oxidized lipids. To test this idea, two lipids formed as a result of oxidative processes were tested, PGPC and PazePC. These two lipids were chosen because they are physiologically relevant and produced under oxidative stress *in vivo*. Both lipids contain a carboxylate by which arginine residues can potentially interact electrostatically (42). Finally, they are relatively water-soluble and can equilibrate between the aqueous phase and cell membranes when added to growth media. When tested with live cells, both PGPC and PazePC enabled the translocation of TMR-r13. In principle, addition of these lipids can have numerous effects and, as noted above, influence cell penetration directly and indirectly. However, these lipids also mediated the partitioning of TMR-r13 into hexane, a solvent of low dielectric constant that mimics the hydrophobic environment of a lipid bilayer. Together, these data show that TMR-r13 binds PGPC and PazePC and that lipid and peptide form structures that can exist in a hydrophobic environment (*e.g.* inverted micelles). In principle, these oxidized lipid species are therefore capable of transporting polyarginine peptides across membranes by direct interactions. Overall, we propose that oxidized lipids with similar properties to PGPC and PazePC might act as direct mediators of membrane translocation. Based on the aforementioned chemical complexity intrinsic to the process of membrane oxidation, this could include a broad variety of species that work in concert to facilitate peptide transport.

Taken together, our results support a plausible model for cytosolic penetration where arginine-rich peptides translocate across the plasma membrane of cells by interacting with anionic lipids present on the cell surface as a result of oxidative stress (Fig. 7, the whisker model is used to represent oxidized lipids containing shortened anionic fatty acyl chains exposed on the surface of the bilayer) (64). Oxidative conditions, including high oxygen concentration, presence of oxidants, or lack of antioxidants, increase the number of oxidized lipids present on the cell surface by a number of mechanisms (54). In one scenario (represented in Fig. 7), anionic oxidized lipids, including anionic oxidized phosphatidylcholine species, directly recruit

cationic CPPs to the cell surface and mediate the transfer of the peptide across the bilayer by formation of structures such as inverted micelles. This model is consistent with previously proposed translocation models involving inverted micelles composed of other anionic species (23, 26, 44, 65, 66). An important distinction, however, is that membrane oxidation is a key variable that can explain how anionic lipids are presented on the cell surface. Alternatively, it is possible that CPPs also exploit hydrophobic or hydrophilic defects present in the bilayer (*e.g.* changes in membrane fluidity and lipid packing) known to increase the permeabilization of oxidized membranes (33, 34). Such effects could in principle synergize with inverted micelle formation and further facilitate translocation.

The intricate interplay between cytosolic penetration and oxidation identified herein should have immediate implications. For instance, using formulations that include CPPs and mildly oxidizing additives might represent a novel strategy to improve the cell permeability of peptides. In addition, by identifying some of the critical parameters that modulate penetration efficacies in tissue cultures, our results should provide a novel consensus for CPP evaluation. For instance, it is clear that the evaluation of cell delivery activities should be performed under defined cellular oxidation states so as to obtain reproducible outcomes. Controlling the cellular oxidation state should also be important when comparing various CPPs or when using tissue cultures as predictive models of *in vivo* behavior (*i.e.* the 20% oxygen condition used in tissue cultures might be relevant to airway epithelium *in vivo,* whereas the 2% oxygen condition is presumably more relevant to the *in vivo* oxygen tension experienced by other tissues).

Author Contributions—T. Y. W. and J. P. P. designed the experiments. T. Y. W. and Y. S. generated and processed the data. T. Y. W., Y. S., N. M., A. E. O., and K. N. contributed the reagents. T. Y. W. and J. P. P. wrote the manuscript. All authors reviewed the results and approved the final version of the manuscript.

Acknowledgments—We thank J. Sacchettini (Texas A&M University) for HDF cells and E. Shoubridge (Montreal Neurological Institute and Hospital) for MCH58 cells. We also thank Professors S. Lockless, C. Kaplan, and T. Meek for critically reading the manuscript.

References

1. Chu, Q., Moellering, R. E., Hilinski, G. J., Kim, Y. W., Grossmann, T. N., Yeh, J. T., and Verdine, G. L. (2015) Towards understanding cell penetration by stapled peptides. *Medchemcomm.* **6,** 111–119
2. Verdine, G. L., and Hilinski, G. J. (2012) Stapled peptides for intracellular drug targets. *Methods Enzymol.* **503,** 3–33
3. Qian, Z., Liu, T., Liu, Y. Y., Briesewitz, R., Barrios, A. M., Jhiang, S. M., and Pei, D. (2013) Efficient delivery of cyclic peptides into mammalian cells with short sequence motifs. *ACS Chem. Biol.* **8,** 423–431
4. Mandal, D., Nasrolahi Shirazi, A., and Parang, K. (2011) Cell-penetrating homochiral cyclic peptides as nuclear-targeting molecular transporters. *Angew. Chem. Int. Ed. Engl.* **50,** 9633–9637
5. Cascales, L., Henriques, S. T., Kerr, M. C., Huang, Y. H., Sweet, M. J., Daly, N. L., and Craik, D. J. (2011) Identification and characterization of a new family of cell-penetrating peptides: cyclic cell-penetrating peptides. *J. Biol. Chem.* **286,** 36932–36943
6. Lättig-Tünnemann, G., Prinz, M., Hoffmann, D., Behlke, J., Palm-Apergi, C., Morano, I., Herce, H. D., and Cardoso, M. C. (2011) Backbone rigidity and static presentation of guanidinium groups increases cellular uptake of arginine-rich cell-penetrating peptides. *Nat. Commun.* **2,** 453
7. Wender, P. A., Mitchell, D. J., Pattabiraman, K., Pelkey, E. T., Steinman, L., and Rothbard, J. B. (2000) The design, synthesis, and evaluation of molecules that enable or enhance cellular uptake: peptoid molecular transporters. *Proc. Natl. Acad. Sci. U.S.A.* **97,** 13003–13008
8. Peretto, I., Sanchez-Martin, R. M., Wang, X. H., Ellard, J., Mittoo, S., and Bradley, M. (2003) Cell penetrable peptoid carrier vehicles: synthesis and evaluation. *Chem. Commun.* **18,** 2312–2313
9. Schröder, T., Schmitz, K., Niemeier, N., Balaban, T. S., Krug, H. F., Schepers, U., and Bräse, S. (2007) Solid-phase synthesis, bioconjugation, and toxicology of novel cationic oligopeptoids for cellular drug delivery. *Bioconjug. Chem.* **18,** 342–354
10. Xiao, X., Yu, P., Lim, H. S., Sikder, D., and Kodadek, T. (2007) A cell-permeable synthetic transcription factor mimic. *Angewandte Chemie* **46,** 2865–2868
11. Kwon, Y. U., and Kodadek, T. (2007) Quantitative evaluation of the relative cell permeability of peptoids and peptides. *J. Am. Chem. Soc.* **129,** 1508–1509
12. Milletti, F. (2012) Cell-penetrating peptides: classes, origin, and current landscape. *Drug Discov. Today* **17,** 850–860
13. Dietz, G. P., and Bähr, M. (2004) Delivery of bioactive molecules into the cell: the Trojan horse approach. *Mol. Cell. Neurosci.* **27,** 85–131
14. Lehto, T., Kurrikoff, K., and Langel, Ü. (2012) Cell-penetrating peptides for the delivery of nucleic acids. *Expert Opin. Drug Deliv.* **9,** 823–836
15. Kosuge, M., Takeuchi, T., Nakase, I., Jones, A. T., and Futaki, S. (2008) Cellular internalization and distribution of arginine-rich peptides as a function of extracellular peptide concentration, serum, and plasma membrane associated proteoglycans. *Bioconjug. Chem.* **19,** 656–664
16. Duchardt, F., Fotin-Mleczek, M., Schwarz, H., Fischer, R., and Brock, R. (2007) A comprehensive model for the cellular uptake of cationic cell-penetrating peptides. *Traffic* **8,** 848–866
17. Jiao, C. Y., Delaroche, D., Burlina, F., Alves, I. D., Chassaing, G., and Sagan, S. (2009) Translocation and endocytosis for cell-penetrating peptide internalization. *J. Biol. Chem.* **284,** 33957–33965
18. Hirose, H., Takeuchi, T., Osakada, H., Pujals, S., Katayama, S., Nakase, I., Kobayashi, S., Haraguchi, T., and Futaki, S. (2012) Transient focal membrane deformation induced by arginine-rich peptides leads to their direct penetration into cells. *Mol. Ther.* **20,** 984–993
19. Wadia, J. S., Stan, R. V., and Dowdy, S. F. (2004) Transducible TAT-HA fusogenic peptide enhances escape of TAT-fusion proteins after lipid raft macropinocytosis. *Nat. Med.* **10,** 310–315
20. Erazo-Oliveras, A., Najjar, K., Dayani, L., Wang, T. Y., Johnson, G. A., and Pellois, J. P. (2014) Protein delivery into live cells by incubation with an endosomolytic agent. *Nat. Methods* **11,** 861–867
21. Madani, F., Lindberg, S., Langel, U., Futaki, S., and Gräslund, A. (2011) Mechanisms of cellular uptake of cell-penetrating peptides. *J. Biophys.* **2011,** 414729
22. Erazo-Oliveras, A., Muthukrishnan, N., Baker, R., Wang, T.-Y., and Pellois, J.-P. (2012) Improving the endosomal escape of cell-penetrating peptides and their cargos: strategies and challenges. *Pharmaceuticals* **5,** 1177–1209
23. Derossi, D., Calvet, S., Trembleau, A., Brunissen, A., Chassaing, G., and Prochiantz, A. (1996) Cell internalization of the third helix of the Antennapedia homeodomain is receptor-independent. *J. Biol. Chem.* **271,** 18188–18193
24. Wender, P. A., Galliher, W. C., Goun, E. A., Jones, L. R., and Pillow, T. H. (2008) The design of guanidinium-rich transporters and their internalization mechanisms. *Adv. Drug Deliv. Rev.* **60,** 452–472
25. Lamazière, A., Burlina, F., Wolf, C., Chassaing, G., Trugnan, G., and Ayala-Sanmartin, J. (2007) Non-metabolic membrane tubulation and permeability induced by bioactive peptides. *PLoS One* **2,** e201
26. Herce, H. D., Garcia, A. E., and Cardoso, M. C. (2014) Fundamental molecular mechanism for the cellular uptake of guanidinium-rich molecules. *J. Am. Chem. Soc.* **136,** 17459–17467
27. Deshayes, S., Plénat, T., Charnet, P., Divita, G., Molle, G., and Heitz, F. (2006) Formation of transmembrane ionic channels of primary amphipathic cell-penetrating peptides. Consequences on the mechanism of

cell penetration. *Biochim. Biophys. Acta* **1758,** 1846–1851
28. Yandek, L. E., Pokorny, A., Florén, A., Knoelke, K., Langel, U., and Almeida, P. F. (2007) Mechanism of the cell-penetrating peptide transportan 10 permeation of lipid bilayers. *Biophys. J.* **92,** 2434–2444
29. Verdurmen, W. P., Thanos, M., Ruttekolk, I. R., Gulbins, E., and Brock, R. (2010) Cationic cell-penetrating peptides induce ceramide formation via acid sphingomyelinase: implications for uptake. *J. Control. Release* **147,** 171–179
30. Halliwell, B. (2003) Oxidative stress in cell culture: an under-appreciated problem? *FEBS Lett.* **540,** 3–6
31. Halliwell, B. (2014) Cell culture, oxidative stress, and antioxidants: avoiding pitfalls. *Biomed. J.* **37,** 99–105
32. Israël, N., and Gougerot-Pocidalo, M. A. (1997) Oxidative stress in human immunodeficiency virus infection. *Cell. Mol. Life Sci.* **53,** 864–870
33. Kotova, E. A., Kuzevanov, A. V., Pashkovskaya, A. A., and Antonenko, Y. N. (2011) Selective permeabilization of lipid membranes by photodynamic action via formation of hydrophobic defects or pre-pores. *Biochim. Biophys. Acta* **1808,** 2252–2257
34. Vernier, P. T., Levine, Z. A., Wu, Y. H., Joubert, V., Ziegler, M. J., Mir, L. M., and Tieleman, D. P. (2009) Electroporating fields target oxidatively damaged areas in the cell membrane. *PLoS One* **4,** e7966
35. Muthukrishnan, N., Donovan, S., and Pellois, J. P. (2014) The photolytic activity of polyarginine cell penetrating peptides conjugated to carboxytetramethylrhodamine is modulated by arginine residue content and fluorophore conjugation site. *Photochem. Photobiol.* **90,** 9
36. Jiang, N., Bénard, C. Y., Kébir, H., Shoubridge, E. A., and Hekimi, S. (2003) Human CLK2 links cell cycle progression, apoptosis, and telomere length regulation. *J. Biol. Chem.* **278,** 21678–21684
37. Babich, H., Liebling, E. J., Burger, R. F., Zuckerbraun, H. L., and Schuck, A. G. (2009) Choice of DMEM, formulated with or without pyruvate, plays an important role in assessing the *in vitro* cytotoxicity of oxidants and prooxidant nutraceuticals. *In Vitro Cell. Dev. Biol. Anim.* **45,** 226–233
38. Howard, A. C., McNeil, A. K., and McNeil, P. L. (2011) Promotion of plasma membrane repair by vitamin E. *Nat. Commun.* **2,** 597
39. Frikke-Schmidt, H., and Lykkesfeldt, J. (2010) Keeping the intracellular vitamin C at a physiologically relevant level in endothelial cell culture. *Anal. Biochem.* **397,** 135–137
40. Saito, Y., Yoshida, Y., Akazawa, T., Takahashi, K., and Niki, E. (2003) Cell death caused by selenium deficiency and protective effect of antioxidants. *J. Biol. Chem.* **278,** 39428–39434
41. Chikazawa, M., Otaki, N., Shibata, T., Miyashita, H., Kawai, Y., Maruyama, S., Toyokuni, S., Kitaura, Y., Matsuda, T., and Uchida, K. (2013) Multispecificity of immunoglobulin M antibodies raised against advanced glycation end products: involvement of electronegative potential of antigens. *J. Biol. Chem.* **288,** 13204–13214
42. Sakai, N., and Matile, S. (2003) Anion-mediated transfer of polyarginine across liquid and bilayer membranes. *J. Am. Chem. Soc.* **125,** 14348–14356
43. Huotari, J., and Helenius, A. (2011) Endosome maturation. *EMBO J.* **30,** 3481–3500
44. Kawamoto, S., Miyakawa, T., Takasu, M., Morikawa, R., Oda, T., Saito, H., Futaki, S., and Nagao, H. (2012) Cell-penetrating peptide induces various deformations of lipid bilayer membrane: Inverted micelle, double bilayer, and transmembrane. *Int. J. Quantum Chem.* **112,** 178–183
45. Long, L. H., and Halliwell, B. (2009) Artefacts in cell culture: pyruvate as a scavenger of hydrogen peroxide generated by ascorbate or epigallocatechin gallate in cell culture media. *Biochem. Biophys. Res. Commun.* **388,** 700–704
46. Kim, D., Kim, C. H., Moon, J. I., Chung, Y. G., Chang, M. Y., Han, B. S., Ko, S., Yang, E., Cha, K. Y., Lanza, R., and Kim, K. S. (2009) Generation of human induced pluripotent stem cells by direct delivery of reprogramming proteins. *Cell Stem Cell* **4,** 472–476
47. Ramakrishna, S., Kwaku Dad, A. B., Beloor, J., Gopalappa, R., Lee, S. K., and Kim, H. (2014) Gene disruption by cell-penetrating peptide-mediated delivery of Cas9 protein and guide RNA. *Genome Res.* **24,** 1020–1027
48. Liu, J., Gaj, T., Patterson, J. T., Sirk, S. J., and Barbas, C. F., 3rd (2014) Cell-penetrating peptide-mediated delivery of TALEN proteins via bioconjugation for genome engineering. *PLoS One* **9,** e85755
49. Drummen, G. P., van Liebergen, L. C., Op den Kamp, J. A., and Post, J. A. (2002) C11-BODIPY(581/591), an oxidation-sensitive fluorescent lipid peroxidation probe: (micro)spectroscopic characterization and validation of methodology. *Free Radic. Biol. Med.* **33,** 473–490
50. Takahashi, M., Shibata, M., and Niki, E. (2001) Estimation of lipid peroxidation of live cells using a fluorescent probe, diphenyl-1-pyrenylphosphine. *Free Radic. Biol. Med.* **31,** 164–174
51. Friedman, P., Horkko, S., Steinberg, D., Witztum, J. L., and Dennis, E. A. (2002) Correlation of antiphospholipid antibody recognition with the structure of synthetic oxidized phospholipids. Importance of Schiff base formation and aldol condensation. *J. Biol. Chem.* **277,** 7010–7020
52. Ingólfsson, H. I., Melo, M. N., van Eerden, F. J., Arnarez, C., Lopez, C. A., Wassenaar, T. A., Periole, X., de Vries, A. H., Tieleman, D. P., and Marrink, S. J. (2014) Lipid organization of the plasma membrane. *J. Am. Chem. Soc.* **136,** 14554–14559
53. Shaw, P. X., Hörkkö, S., Chang, M.-K., Curtiss, L. K., Palinski, W., Silverman, G. J., and Witztum, J. L. (2000) Natural antibodies with the T15 idiotype may act in atherosclerosis, apoptotic clearance, and protective immunity. *J. Clin. Invest.* **105,** 1731–1740
54. Bochkov, V. N., Oskolkova, O. V., Birukov, K. G., Levonen, A. L., Binder, C. J., and Stöckl, J. (2010) Generation and biological activities of oxidized phospholipids. *Antioxid. Redox Signal.* **12,** 1009–1059
55. Falanga, V., and Kirsner, R. S. (1993) Low oxygen stimulates proliferation of fibroblasts seeded as single cells. *J. Cell. Physiol.* **154,** 506–510
56. Packer, L., and Fuehr, K. (1977) Low oxygen concentration extends the lifespan of cultured human diploid cells. *Nature* **267,** 423–425
57. de la Haba, C., Palacio, J. R., Martínez, P., and Morros, A. (2013) Effect of oxidative stress on plasma membrane fluidity of THP-1 induced macrophages. *Biochim. Biophys. Acta* **1828,** 357–364
58. Benderitter, M., Vincent-Genod, L., Pouget, J. P., and Voisin, P. (2003) The cell membrane as a biosensor of oxidative stress induced by radiation exposure: a multiparameter investigation. *Radiat. Res.* **159,** 471–483
59. Melikov, K., Hara, A., Yamoah, K., Zaitseva, E., Zaitsev, E., and Chernomordik, L. V. (2015) Efficient entry of cell-penetrating peptide nona-arginine into adherent cells involves a transient increase in intracellular calcium. *Biochem. J.* **471,** 221–230
60. Volinsky, R., Cwiklik, L., Jurkiewicz, P., Hof, M., Jungwirth, P., and Kinnunen, P. K. (2011) Oxidized phosphatidylcholines facilitate phospholipid flip-flop in liposomes. *Biophys. J.* **101,** 1376–1384
61. Porter, N. A., Caldwell, S. E., and Mills, K. A. (1995) Mechanisms of free radical oxidation of unsaturated lipids. *Lipids* **30,** 277–290
62. Davies, K. J. (2000) Oxidative stress, antioxidant defenses, and damage removal, repair, and replacement systems. *IUBMB Life* **50,** 279–289
63. Takeuchi, T., Kosuge, M., Tadokoro, A., Sugiura, Y., Nishi, M., Kawata, M., Sakai, N., Matile, S., and Futaki, S. (2006) Direct and rapid cytosolic delivery using cell-penetrating peptides mediated by pyrenebutyrate. *ACS Chem. Biol.* **1,** 299–303
64. Greenberg, M. E., Li, X. M., Gugiu, B. G., Gu, X., Qin, J., Salomon, R. G., and Hazen, S. L. (2008) The lipid whisker model of the structure of oxidized cell membranes. *J. Biol. Chem.* **283,** 2385–2396
65. Kawamoto, S., Takasu, M., Miyakawa, T., Morikawa, R., Oda, T., Futaki, S., and Nagao, H. (2011) Inverted micelle formation of cell-penetrating peptide studied by coarse-grained simulation: importance of attractive force between cell-penetrating peptides and lipid head group. *J. Chem. Physics* **134,** 095103
66. Swiecicki, J. M., Bartsch, A., Tailhades, J., Di Pisa, M., Heller, B., Chassaing, G., Mansuy, C., Burlina, F., and Lavielle, S. (2014) The efficacies of cell-penetrating peptides in accumulating in large unilamellar vesicles depend on their ability to form inverted micelles. *Chembiochem* **15,** 884–891